Low-order adaptive deformable mirror

J. Christopher Dainty, Alexander V. Koryabin, and Alexis V. Kudryashov

We report the main parameters of a nine-electrode bimorph piezoelectric adaptive mirror designed to correct low-order aberrations. We describe measurements of the control coefficients for defocus, astigmatism, pure coma, and spherical aberration of this mirror and the temperature stability of its profile. The performance of a simple adaptive optical system for imaging through laboratory-generated turbulence is investigated. This low-order device is suitable for small (<1-m-diameter) telescopes and for nonastronomical applications of adaptive optics. © 1998 Optical Society of America

OCIS code: 350.1260.

1. Introduction

Much of the progress in adaptive optics is associated with increasing the number of subapertures. Systems for astronomical imaging with more than 200 elements have been constructed, and those with many more elements are planned.[1,2] Such systems are inherently expensive because of their large space–bandwidth products. However, the largest low-order phase distortions are rather slow in comparison with high-order ones,[3] and it may be cost effective to use more than one adaptive mirror: one comparatively slow modal mirror with a large range of surface deformation and a second, faster, segmented or continuous face sheet mirror to correct short-scale high-order aberrations. There are many other potential applications of adaptive optics, such as retinal imaging and intracavity high-power laser beam control,[4] that might benefit from low-order, low-cost adaptive optics.

It is well known from the study by Noll[5] that, for Kolmogorov turbulence, approximately 87% of the piston-subtracted wave front variance is due to tilt; the next most important Zernike terms are focus (2.2%), astigmatism (2.2% in each), coma (1.2% in each), and spherical (0.2%), with approximately 3.7% being in the remaining terms. The total phase variance σ_φ^2 is 1.03 $(D/r_0)^{5/3}$, and Strehl ratio $S = \exp(-\sigma_\varphi^2)$, where D is the diameter of the receiving aperture and r_0 is the Fried parameter.[6] Table 1 lists the wave-front variance σ_φ^2 as a function of (D/r_0), together with the Strehl ratios for no correction, correction for tilt, focus, and astigmatism, and correction for all terms up to and including primary spherical aberration. For example, for $(D/r_0) = 5$, full correction of all terms up to primary spherical aberration gives a Strehl ratio of approximately 0.75, close to the Maréchal criterion of a high-quality imaging system. Given that, in the visible, $r_0 \approx 10$–20 cm, these values show that compensation of the second-order aberrations can significantly improve the image quality for 1-m-class telescopes.

For the same values of (D/r_0) we can estimate the required deformation Δx of the adaptive mirror surface to correct these second-order aberrations, as shown in Table 2. In these calculations we used the relation $\Delta x \approx \lambda/2\pi 3\sigma_\varphi$, where λ is the wavelength, set equal to 0.5 mm, and we assume 3-σ limits in a Gaussian distribution. For low-order aberrations other than tilt, the deviation required is less than 1 mm for $(D/r_0) < 10$.

One suitable device for low-order wave-front correction is a bimorph mirror. Recent results have demonstrated the practicality of such devices for astronomy.[7,8] In this paper we describe the performance of a nine-electrode bimorph mirror and describe its use in a simple closed-looped system.

2. Bimorph Deformable Mirror

Bimorph deformable mirrors (BDM's) are described in Refs. 9–13. Our device, manufactured at the International Laser Centre, Moscow, is shown in Fig. 1. It consists of a glass plate firmly glued to a plate actuator disk made from piezoelectric ceramic (piezo-

J. C. Dainty is with the Blackett Laboratory, Imperial College, London SW7 2BZ, UK. A. V. Koryabin is with the International Laser Centre, Moscow State University, Vorobyovy Gory, Moscow 119899, Russia. A. V. Kudryashov is with the Scientific Research Centre for Technological Lasers, Pionerskaya 2, Troytsk 142092, Russia.

Received 31 March 1998.
0003-6935/98/214663-06$15.00/0

Table 1. Strehl Ratios for Different Values of D/r_0[a]

D/r_0	σ_Φ^2 (rad^2)	Strehl Ratio	Compensated Strehl Ratio	
			T + F + A	T + F + A + C + S
1	1.03	0.598	0.968	0.981
2	3.27	0.194	0.902	0.942
5	15.03	5×10^{-4}	0.623	0.753
10	47.81	4×10^{-11}	0.222	0.417

[a]Column 3 gives the Strehl ratio for an uncorrected system, column 4 that for first order tilt (T), focus (F), and astigmatism (A), and column 5 that for these aberrations plus primary coma (C) and spherical aberration (S).

ceramic). The actuator disk consists of two piezoceramic (lead zirconium titanate; PZT) disks soldered together and polarized normally to their surfaces. The thickness of each piezoceramic disk is 0.35 mm. The glass plate is 39 mm in diameter and 2.5 mm thick. The active surface of the plate has a reflecting aluminum layer with a protective SiO_2 overcoat.

For astronomical telescopes of the Cassegrain type with a central obscuration, the mirror can be supported on a central pole. For this purpose a glass tube is attached to the actuator disk. The other end of this tube is glued to a base plate fixed in the mirror mount. This mount has no tip-tilt controlled actuators, so to compensate for wave-front tip-tilt we use a special corrector with a light-weight small (25-mm-diameter) mirror controlled by two piezoceramic stack actuators.

Table 2. Required Profile Deformations Δx (in μm, for 95% Probability of Correction)

Type of Deformation	Δx			
	$D/r_0 = 1$	$D/r_0 = 2$	$D/r_0 = 5$	$D/r_0 = 10$
Total	0.97	1.73	3.71	6.6
Tilt	0.9	1.61	3.45	6.14
Focus, astigmatism	0.15	0.26	0.56	0.99
Pure coma	0.11	0.19	0.41	0.73
Spherical	0.05	0.08	0.18	0.32

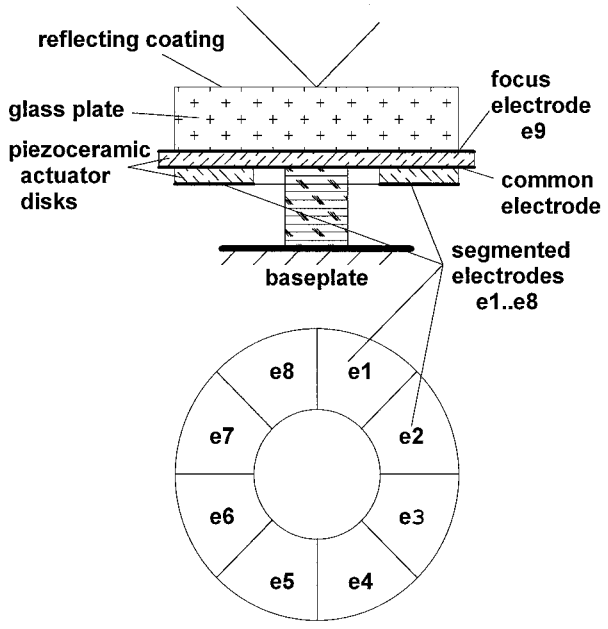

Fig. 1. Nine-element bimorph deformable mirror.

Table 3. Control Voltage Sign on Each Electrode

Aberration	e1	e2	e3	e4	e5	e6	e7	e8	e9
Defocus (by e9)									±
Defocus (by e1–e8)	±	±	±	±	±	±	±	±	
Astigmatism I	+		−		+		−		
Astigmatism II		+		−		+		−	
Spherical	+	+	+	+	+	+	+	+	−

The interface between the two disks contains a continuously conducting ground electrode. Another continuously conducting electrode (e9) between the actuator and the glass plate is used to control the curvature of the whole mirror and is referred to as the general focus electrode. The outer surface of the actuator has eight separate ring-segment electrodes, e1–e8. The dependence of the mirror profile on control voltages applied to electrodes can be described by the Poisson equation.[11] The geometry of the electrodes was designed especially to control second-order aberrations and spherical aberration. To minimize the number of control circuits, opposite segmented electrodes can be connected into pairs, so we need only five outputs to control general focus and astigmatism. To control second-order and spherical aberration we apply control voltages as shown in Table 3.

3. Parameters of the Mirror

The spatial parameters of the mirror were measured with a phase-shifting interferometer (Moller–Wedel) with appropriate software (Phase Shift Technology). To apply arbitrary voltages to the mirror electrodes we used a simple manual control unit with nine output voltages up to ±150 V. The interferograms of some mirror profiles are shown in Fig. 2. The mirror profile's controllability can be described in terms of the control coefficient $k = \Delta A/\Delta U$, where ΔA is the peak-to-peak value of aberration profile (in micrometers) and ΔU is the control voltage applied (in volts). The main spatial parameters of the mirror are shown in Table 4, which lists the control coefficients k, the relative rms error of aberration fitting, and the peak-to-peak aberration deformation. It should be pointed out that the response function of every electrode of this corrector is the modal one, meaning that by applying voltage to a given element we get the deformation of the whole mirror surface. This result on the one hand complicates the process of mirror control but at the same time reduces the number of elements that need to be used to correct low-order aberrations.

The mirror was not optimally designed to correct the coma, so we calculated the control coefficient for coma by the following procedure: For every seg-

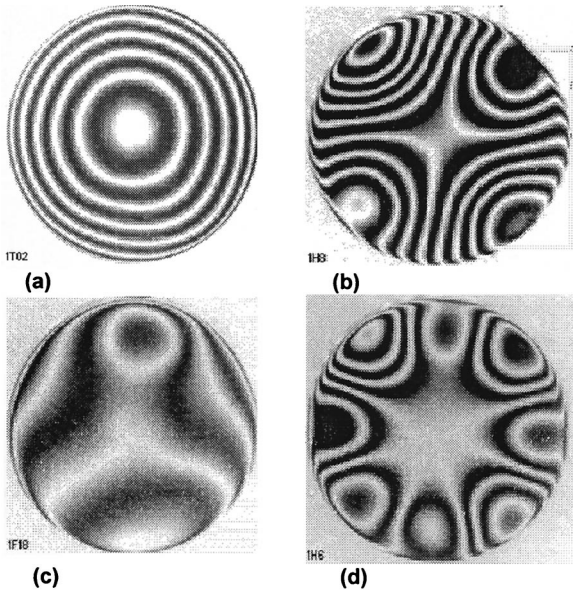

Fig. 2. Interferometric profiles of the mirror at $\lambda = 0.63$ μm: (a) defocus (+30 V to electrode e9), (b) one electrode profile (+60 V to electrode e1), (c) astigmatism, (d) profile for +120 V at odd electrodes and +120 V at even ones.

mented electrode we measured the response profile and its Zernike expansion (36 terms) that were used in calculating the control coefficient and the accuracy of the lowest aberration coefficients by the least-squares method. As a result, one of the coma terms can be fitted with a rms error of less than 5%, whereas the other has a significantly higher fitting error, 15% in rms terms. The fitting-error value obtained for spherical aberration is ~30%. At the same time, fitting errors for the second-order aberrations are small: ~3% for astigmatism and ~0.6% for defocus.

The PZT material of the mirror actuators exhibits significant hysteresis. The typical hysteresis curve for the general focus voltage is shown in Fig. 3. In all cases the relative value for the hysteresis curve width does not exceed 11%.

Knowledge of the temperature dependence of the aberration control coefficients is of great importance for real applications. A simple fan heater was used to increase the temperature by several degrees centigrade in the room where interferometer was installed. A thermocouple (Thandar TH302; precision, 0.1 °C was attached to the mirror mount. The measurements show a significant temperature dependence of focus on the difference in temperature expansion coefficients of the glass and the piezoceramics that we used to fabricate the mirror. The dependence of temperature on the aberrations is shown in Fig. 4, and the temperature coefficients $m = \Delta A/\Delta T$ are listed in the rightmost column in Table 4: This information was extracted from the data by a linear least-squares approximation. The largest m value is for defocus: $m = 0.38$ μm/°C; coefficients for other low-order aberrations are 10–30 times less. The sensitivity of focus to temperature is a significant

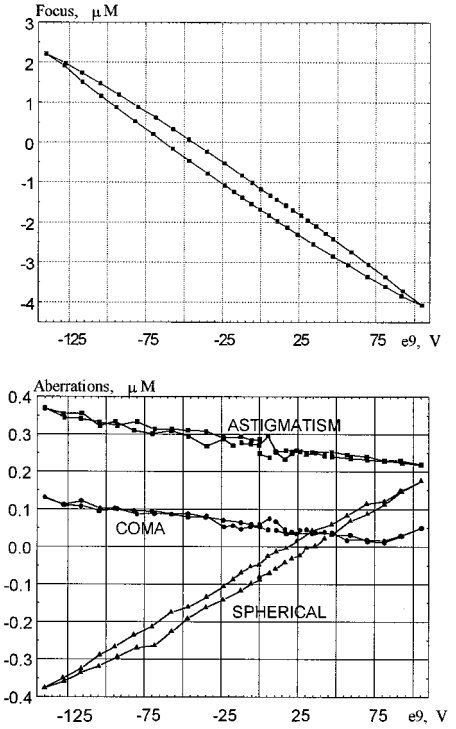

Fig. 3. Dependence of aberrations on the voltage on general focus electrode e9.

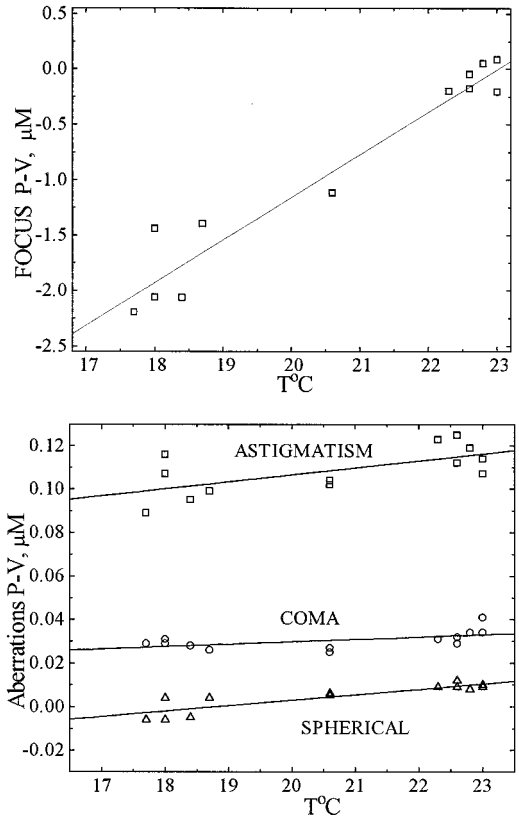

Fig. 4. Temperature dependencies of the lowest-order aberrations.

Table 4. Main Spatial Parameters of the Mirror

Aberration	$k \times 10^2$ (μm/V)	Peak-to-Peak Value at 200 V (μm)	Fitting rms Peak to Peak (%)	m (μm/1 °C)
Focus	2.56 (by e9 control)	5.1	0.6	0.38
	1.12 (by e1–e8 control)	2.2		
Astigmatism	2.06	4.1	3	0.003
Pure coma	0.51 (calculated)	1	5, 15	0.0011
Spherical	0.1	0.2	30	0.0025

(negative) feature of this bimorph mirror, but the range of aberration control for this mirror is high enough to correct turbulence-induced distortions and to compensate for its own thermal distortions over 10–15 °C variations of temperature.

The flatness of the mirror, i.e., aberrations with all electrodes connected to ground, cannot be described unless the temperature dependence is taken into account. At 18 °C, the peak-to-peak total mirror deformation is 1.5 μm, or 0.39 μm rms. The main part of the deformation is due to defocus (1.35 μm); second-order plus pure coma and spherical aberrations produce 99.86% of the total deformation rms. By applying relatively small control voltages (16.4 V maximum value for e4 = e8) we succeeded in fitting a plane with 0.033-μm rms and 0.1-μm peak-to-peak deformation. These results turned out to be in good accordance with calculations of the plane fitting errors, based on the measured spatial response functions.

The resonance frequencies of the mirror were measured with the help of a Kenwood AG-204 oscillator, an ISO-Tech ISR-620 oscilloscope, and a Black Star Apollo-10 frequency meter. During the measurements we connected driving sine voltage to the X input of the oscilloscope as well as to the frequency meter while the signal was measured at the Y input of the oscilloscope. This procedure enabled us to use both phase and amplitude measurements of resonances, which was more precise than measuring only the amplitude measurement. A typical frequency-response curve is shown in Fig. 5.

4. Low-Order Experimental Optical System

The mirror was tested in a simple adaptive optical system for imaging through laboratory-generated turbulence. The experimental setup is shown in Fig. 6. A He–Ne laser beam was expanded from ≈1 mm to 10 mm in diameter by lenses L1 and L2 and directed into a glass water cell (wc), which was used to produce turbulent distortions of the wave front. The turbulence was produced by the convection movement of water between the lower hot metal plate and the cold plate placed at the top of the cell; the length of the water cell was 34 cm. The temperature difference between the cold and the hot plates was 5–7 °C and produced a C_n^2 of approximately 0.28×10^{-8} cm$^{-2/3}$ and r_0 of 0.5–0.8 mm. Diaphragms D1 and D2 define the beam diameter.

After reflecting from tip-tilt controlled mirror M1, the laser beam went through beam splitter S and a telescope system made of lenses L4 and L5 to bimorph mirror BM. The beam width on the adaptive mirror was approximately 35 mm. The reflected laser beam was directed by a beam splitter to the measurement arm. We used lens L3 (with focus 200 mm), 25-μm pinhole D3, and photodiode PD to measure the Strehl intensity of the corrected beam. The signal from the photodiode went through a dc amplifier A and into a 486 personal computer. The maximum rate of analog-to-digital conversion was 25 kHz.

To control the profile of the bimorph mirror we used the parallel interface of the computer together with a digital-to-analog converter unit with ±150-V high-voltage amplifiers. The frequency range of the amplifiers loaded by our mirror was limited to 200 Hz. We used simply a "hill climbing"[14] algorithm to calculate the control signals for maximization of the Strehl intensity.

The optical system that we used had some residual

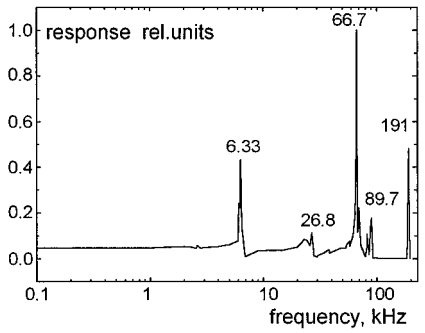

Fig. 5. Typical frequency-response curve.

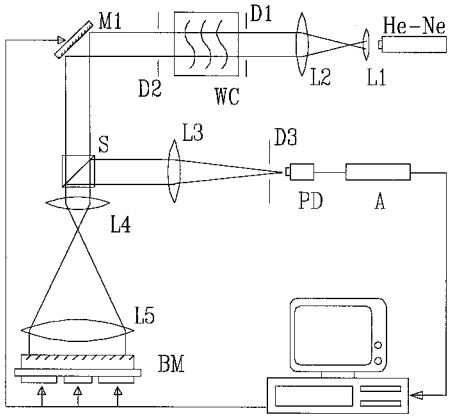

Fig. 6. Low-order adaptive system setup.

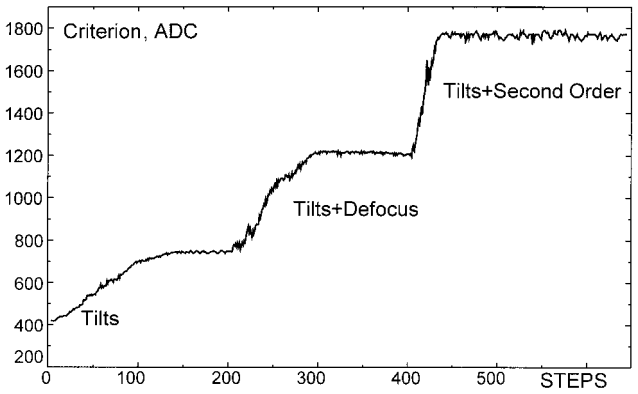

Fig. 7. Correction of static aberrations; ADC, analog-to-digital converter.

aberrations, and these were corrected first as a preliminary test of the system. At the same time we studied the number of steps that the system required to correct such aberrations. To get a more effective result we shifted pinhole D3 slightly along and transverse to the beam propagation to simulate additional defocus and tip-tilt.

A typical time dependence of the photodiode signal during the adaptation process is shown in Fig. 7. As we might expect, the maximum value of the Strehl intensity achieved by adaptation varied as different numbers of aberrations were controlled. The final photodetector values were ~740 (in arbitrary units proportional to intensity) for tip-tilt correction only; 1230 for tip-tilt and defocus correction, and 1760 for tip-tilt, defocus, and astigmatism correction. The initial value was 402 (just before the adaptation process started). It took the system from ~150 steps (for the tip-tilt case) to ~50 steps (for astigmatism control) to achieve the maximum Strehl intensity (1760 in arbitrary units).

The temporal and spatial parameters of the turbulence produced in the water cell are related to each other: When the coherence length r_0 was large the typical value of time scale was large as well, and when the turbulence was rapid the coherence length was small. The typical step time delay in the system caused by the software and hardware delays was ~0.6 ms, but to prevent the resonance excitation of the tip-tilt actuators and the bimorph mirror we imposed an additional programmable delay in the range 1–2 ms.

Figure 8(a) shows the signal from photodiode PD (see Fig. 6) in the presence of the phase distortions caused by the water cell, without any adaptive correction. With the adaptive system operating, the higher amplitude and stability shown in Fig. 8(b) are obtained. In this case a modified gradient method of correction was used, which sometimes had difficulty coping with the more rapid time variability of the turbulence: For a larger temperature difference between the plates and hence a more rapid time variation, a hill-climbing algorithm performs better. Typical values for the Strehl factor before (S_1) and after (S_2) the adaptive system was switched on, defined as $S_{1,2} = I_{1,2}/I_0$, where $I_{1,2}$ is the signal from photodiode PD and I_0, the intensity in the absence of turbulence, were 0.40 and 0.86, a modest increase of a factor of 2. Improved performance would be obtained with dedicated separate signal-processing circuitry for tip-tilt and higher-order corrections and by the use of a quadrant detector for tip-tilt and a low-order Shack–Hartmann or curvature sensor for higher-order aberrations.

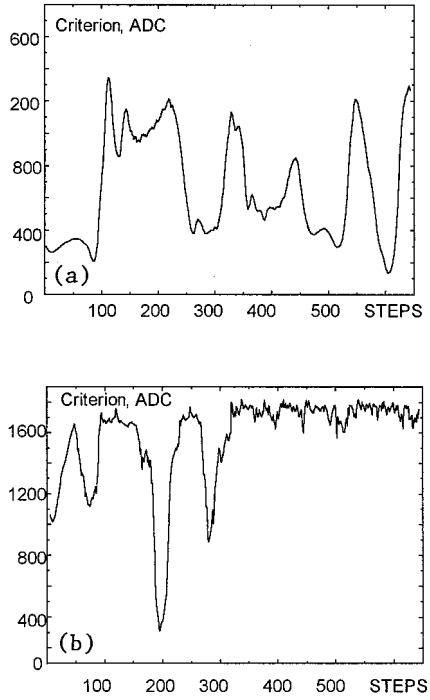

Fig. 8. Time behavior of the Strehl intensity: (a) pure turbulence, (b) partially corrected turbulence; ADC, analog-to-digital converter.

5. Conclusions

The main spatial and temporal parameters of a bimorph mirror were tested. The plane fitting rms error was ~0.033 μm, and deformation for the second-order aberrations was ~4 μm. The typical width of the mirror's actuator hysteresis curve was ~10%. The mirror was tested in a simple adaptive system for compensation of the laboratory-induced turbulence. The performance of this system showed the possibility to improve beam quality in the presence of strong turbulence with D/r_0 values of ≲10, although in this closed-loop system we achieved an increase in the Strehl parameter of only a factor of 2.

The authors thank N. J. Wooder, F. C. Reavell, and A. A. D. Cañas for assistance during mirror and system testing and S. Hanif for electronics support. We also thank A. Bogaturov and V. Myakinin of the Institute of Atmospheric Physics, Moscow, for supplying data on the characteristics of the water cell turbulence. This study was sponsored by the U.S. Air Force European Office of Aerospace Research and Development, London, The Royal Society, and the

Particle Physics and Astronomy Research Council under grant GR/H64156.

References

1. R. Q. Fugate, B. L. Ellerbroek, C. H. Higgins, M. P. Jelonek, W. J. Lange, A. C. Slavin, W. J. Wild, D. M. Winkler, J. M. Wynia, J. M. Spinhire, B. R. Boeke, B. E. Ruane, J. F. Moroney, M. D. Oliker, D. W. Swindle, and R. A. Cleis, "Two generations of laser-guide-star adaptive-optics experiments at the Starfire Optical Range," J. Opt. Soc. Am. A **11,** 310–324 (1994).
2. M. A. Ealey and J. A. Wellman, "Xinetics low cost deformable mirrors with actuator replacement cartridges," in *Adaptive Optics in Astronomy*, M. A. Ealey and F. Merkle, eds., Proc SPIE **2201,** 680–687 (1994).
3. C. B. Hogge and R. R. Butts, "Frequency spectra for the geometric representation of wavefront distortions due to atmospheric turbulence," IEEE Trans. Antennas Propag. **AP-24,** 144–154 (1976).
4. A. V. Kudryashov and V. V. Samarkin, "Control of high-power CO_2-laser beam by adaptive optical elements," Opt. Commun. **118,** 317–322 (1995).
5. R. J. Noll, "Zernike polynomials and atmospheric turbulence," J. Opt. Soc. Am. **66,** 207–211 (1976).
6. D. L. Fried, "Optical resolution through a randomly inhomogeneous medium for very long and very short exposures," J. Opt. Soc. Am. A **56,** 1372–1379 (1966).
7. F. Roddier, "Curvature sensing and compensation: a new concept in adaptive optics," Appl. Opt. **27,** 1223–1225 (1988).
8. F. Forbes, F. Roddier, G. Poczulp, C. Pinches, G. Sweeny, and R. Dueck, "Segmented bimorph deformable mirror," J. Phys. E **22,** 402–405 (1989).
9. N. T. Adelman, "Spherical mirror with piezoelectrically controlled curvature," Appl. Opt. **16,** 3075–3077 (1977).
10. S. A. Kokorowsky, "Analysis of adaptive optical elements made from piezoelectric bimorphs," J. Opt. Soc. Am. **69,** 181–187 (1979).
11. S. G. Lipson and E. Steinhaus, "Bimorph piezoelectric flexible mirror," J. Opt. Soc. Am. **69,** 478–481 (1979).
12. M. A. Vorontsov, A. V. Kudryashov, S. I. Nazarkin, and V. I. Shmalgauzen, "Flexible mirror for adaptive light beam formation systems," Sov. J. Quantum Electron. **14,** 839–841 (1984).
13. C. Schwartz, E. Ribak, and S. G. Lipson, "Bimorph adaptive mirrors and curvature sensing," J. Opt. Soc. Am. A **11,** 895–902 (1994).
14. J. W. Hardy, "Active optics: new technique for light beam control," Proc. IEEE **66,** 651–697 (1978).